Article

Phages reconstitute NAD$^+$ to counter bacterial immunity

https://doi.org/10.1038/s41586-024-07986-w

Received: 8 February 2024

Accepted: 22 August 2024

Published online: 25 September 2024

Check for updates

Ilya Osterman[1]✉, Hadar Samra[1], Francois Rousset[1], Elena Loseva[1], Maxim Itkin[2], Sergey Malitsky[2], Erez Yirmiya[1], Adi Millman[1] & Rotem Sorek[1]✉

Bacteria defend against phage infection through a variety of antiphage defence systems[1]. Many defence systems were recently shown to deplete cellular nicotinamide adenine dinucleotide (NAD$^+$) in response to infection, by cleaving NAD$^+$ into ADP-ribose (ADPR) and nicotinamide[2–7]. It was demonstrated that NAD$^+$ depletion during infection deprives the phage of this essential molecule and impedes phage replication. Here we show that a substantial fraction of phages possess enzymatic pathways allowing reconstitution of NAD$^+$ from its degradation products in infected cells. We describe NAD$^+$ reconstitution pathway 1 (NARP1), a two-step pathway in which one enzyme phosphorylates ADPR to generate ADPR pyrophosphate (ADPR-PP), and the second enzyme conjugates ADPR-PP and nicotinamide to generate NAD$^+$. Phages encoding NARP1 can overcome a diverse set of defence systems, including Thoeris, DSR1, DSR2, SIR2–HerA and SEFIR, all of which deplete NAD$^+$ as part of their defensive mechanism. Phylogenetic analyses show that NARP1 is primarily encoded on phage genomes, suggesting a phage-specific function in countering bacterial defences. A second pathway, NARP2, allows phages to overcome bacterial defences by building NAD$^+$ using metabolites different from ADPR-PP. Our findings reveal a unique immune evasion strategy in which viruses rebuild molecules depleted by defence systems, thus overcoming host immunity.

NAD$^+$ and its reduced form, NADH, are central metabolites essential for numerous core metabolic processes across all domains of life. In most bacteria, NAD$^+$ is an essential cofactor for redox reactions[8], and in the absence of NAD$^+$, pathways such as oxidative phosphorylation[9], amino acid biosynthesis[10] and fatty acid biosynthesis[10] are arrested. NAD$^+$ was also shown to be necessary for post-translational protein modifications[11] and for DNA ligation processes[12].

Recent data show that NAD$^+$ metabolism is central for bacterial defence against phages[1–4]. Specifically, numerous bacterial defence systems were shown to deplete cellular NAD$^+$ once they detect phage infection, thus depleting the cell of energy and impeding phage propagation. Such defence systems include prokaryotic argonautes (pAgo)[2,4], type I Thoeris[3], AVAST[5], CBASS[6], DSR1[2], DSR2[2], SIR2–HerA[2], SEFIR[1] and additional defence systems encoding protein domains associated with NAD$^+$ depletion[7]. A recent analysis of the abundance of defence systems in microbial genomes shows that at least 7% of all sequenced bacterial genomes carry defence systems that cause NAD$^+$ depletion in response to phage infection[1].

Once NAD$^+$-depleting defence systems detect phage infection, they cleave NAD$^+$ into ADPR and nicotinamide[2]. As there is no known cellular pathway that can directly rebuild NAD$^+$ from these molecules, cleaving of NAD$^+$ into ADPR and nicotinamide is an efficient way to deplete NAD$^+$ from infected cells. Depletion of NAD$^+$ during infection was shown to halt phage propagation and, in some cases, cause premature cell lysis[2,3], possibly by activating the lysis machinery of the phage before the completion of the phage cycle[2,13].

Here we show that at least 5% of sequenced phage genomes encode NAD$^+$ reconstitution pathways that allow them to rebuild NAD$^+$ directly from ADPR and nicotinamide. We discover NARP1, a phage-encoded pathway involving two enzymatic reactions that, to our knowledge, have not been described before. We also show that NARP2, an alternative NAD$^+$ reconstitution pathway utilizing classical NAD$^+$-salvage enzymatic reactions, is used by phages to rebuild NAD$^+$ during infection. NAD$^+$ reconstitution pathways allow phages to overcome many NAD$^+$-depleting defence systems irrespective of the mechanism of phage detection and signal transfer in these systems.

A phage operon subverts bacterial defence

While examining the genomes of phages from the BASEL collection[14], we noticed a two-gene operon that recurred in four phages in this set (Fig. 1a and Extended Data Fig. 1a). This operon caught our attention because the Pfam annotations of its two genes suggested involvement in synthesis of biochemical intermediates in the NAD$^+$ biosynthesis pathway. The first gene in this operon was annotated as belonging to the phosphoribosylpyrophosphate (PRPP) synthetase (Prs) gene family (Pfam accession PF14572), and the second gene was annotated as the

[1]Department of Molecular Genetics, Weizmann Institute of Science, Rehovot, Israel. [2]Life Sciences Core Facilities, Weizmann Institute of Science, Rehovot, Israel. ✉e-mail: ilya.osterman@weizmann.ac.il; rotem.sorek@weizmann.ac.il

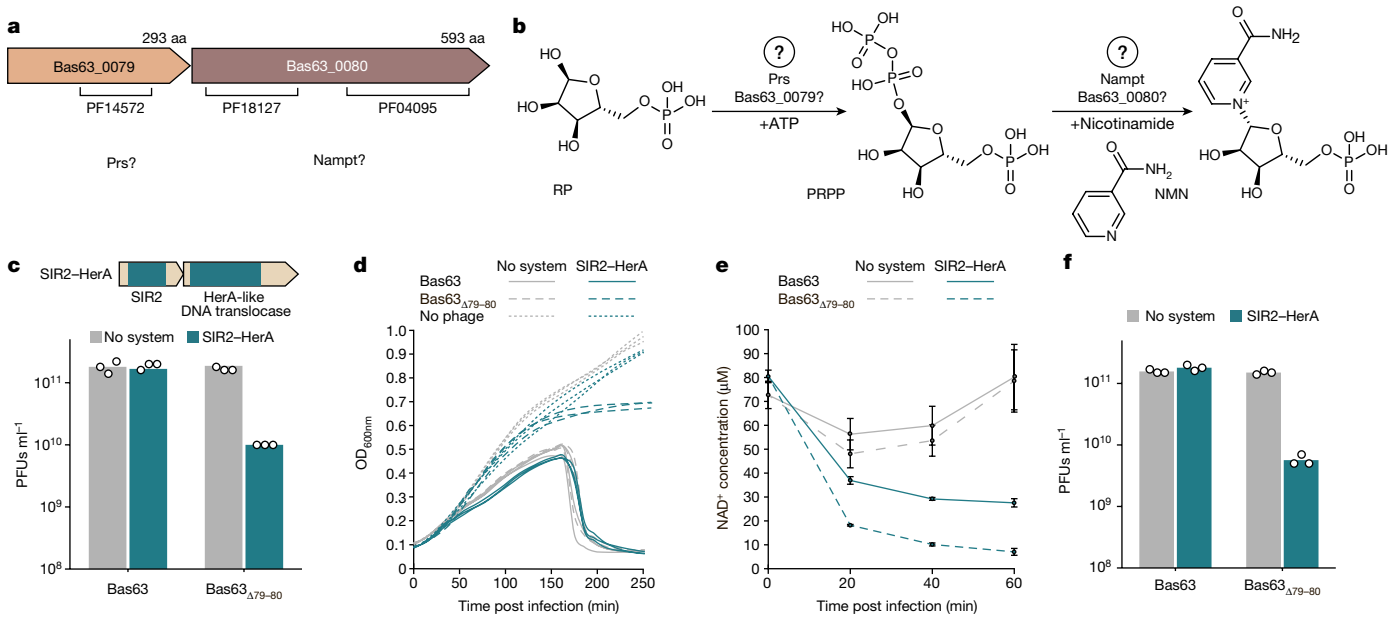

Fig. 1 | A phage-encoded operon that counteracts bacterial NAD$^+$ depletion defence. a, Domain organization of the proteins encoded by genes 79–80 from phage JohannRWettstein (Bas63). Pfam annotations are indicated. aa, amino acids. **b**, The putative enzymatic functions of the phage-encoded proteins according to their predicted protein domains. In this study we show that these predicted reactions are not the actual reactions performed by the phage enzymes. **c**, Operon 79–80 allows phage Bas63 to overcome SIR2–HerA defence. Data represent plaque-forming units (PFUs) per millilitre of wild-type Bas63 and Bas63 in which the two-gene operon was deleted, infecting cells that express the SIR2–HerA defence system or control cells with an empty vector (no system). The bar graph represents the average of three independent replicates, with individual data points overlaid. **d**, Liquid culture growth of *E. coli* cells expressing the SIR2–HerA operon or control strain without defence genes (no system). Cells were infected by phages Bas63 and Bas63$_{\Delta 79-80}$ at a multiplicity of infection (MOI) of 0.01. Data from three replicates are presented as individual curves. OD_{600nm}, optical density at 600 nm. **e**, NAD$^+$ concentration in the lysate of cells expressing SIR2–HerA or control cells with an empty vector instead (no system), infected with phages Bas63 and Bas63$_{\Delta 79-80}$ at MOI = 10. Cells were collected before infection (0 min) and 20, 40 or 60 min after infection. NAD$^+$ concentration in cell lysates was measured by the NAD/NADH-Glo biochemical assay. Data are presented as mean values ± standard deviation (s.d.), $n = 3$ replicates. **f**, Same experiment as in **d**, but on an *E. coli* strain with deletions of the two genes *pncC* and *nadR*.

nicotinamide phosphoribosyltransferase (Nampt) gene (Pfam accessions PF18127 and PF04095; Fig. 1a). In bacteria, Prs enzymes produce PRPP, a biochemical intermediate in the biosynthesis pathway of purine and pyrimidine nucleotides, as well as NAD$^+$. Nampt enzymes utilize PRPP and nicotinamide as substrates to generate nicotinamide mononucleotide (NMN), a molecular moiety that can be used as a precursor for NAD$^+$ biosynthesis through NAD$^+$ salvage pathways (Fig. 1b,c). It was previously shown that genes annotated as Nampt genes are abundant in phage genomes[15,16]. It was further reasoned that phages may utilize NAD$^+$ biosynthesis enzymes to overcome the effects of NAD$^+$-depleting defence systems[15].

To examine the role of the two-gene operon that we detected in BASEL phages, we deleted this operon from the BASEL phage Bas63 (JohannRWettstein[14]). The wild-type Bas63 was able to infect *Escherichia coli* cells encoding the defence system SIR2–HerA (also called Nezha[17]), which is known to deplete NAD$^+$ following phage recognition[2,17] (Fig. 1c). By contrast, a Bas63 strain in which the two-gene operon was deleted formed about 20-fold fewer plaques on agar plates, suggesting that SIR2–HerA defends against the modified phage and that the phage two-gene operon can counter this defence (Fig. 1c). These results were confirmed by infecting cells in liquid culture, with a culture of bacteria encoding the SIR2–HerA defence system collapsing when infected with the wild-type phage, but being able to grow when infected by the phage in which the two genes were deleted (Fig. 1d).

To test whether the two-gene operon allows the phage to overcome the NAD$^+$ depletion effects of SIR2–HerA, we recorded cellular NAD$^+$ levels during infection. NAD$^+$ was strongly depleted in cells expressing SIR2–HerA that were infected by the mutated phage, confirming the activity of SIR2–HerA against this phage (Fig. 1e). When infected with the wild-type Bas63 that encodes the two-gene operon, the observed NAD$^+$ depletion was less marked, showing that this phage can partially overcome SIR2–HerA-mediated NAD$^+$ depletion (Fig. 1e).

Considering the Pfam domain annotations of the proteins encoded by the two phage genes, we expected these genes to produce NMN as their end product (Fig. 1b). There are two NAD$^+$ salvage pathways in *E. coli* that can use NMN to synthesize NAD$^+$, either through the enzyme PncC[18] or through the enzyme NadR[19]. We therefore reasoned that deletion of *pncC* and *nadR* from the *E. coli* genome would render phage Bas63 sensitive to SIR2–HerA defence despite encoding the two anti-defence genes. However, wild-type Bas63 was still able to overcome NAD$^+$-depletion-based defence in a Δ*pncC*Δ*nadR E. coli* strain that encoded SIR2–HerA (Fig. 1f). These results indicated that the mechanism used by Bas63 to counter SIR2–HerA defence does not require the NAD$^+$ salvage pathway naturally encoded by *E. coli*. These data also implied that the Pfam annotations of the two phage proteins might be incorrect, and that these proteins synthesize a molecule other than NMN.

A new pathway for NAD$^+$ synthesis

To gain further insights into the mechanism by which the two phage genes increase NAD$^+$ levels during infection, we used untargeted mass spectrometry (MS) to analyse small metabolites in cells infected with the wild-type Bas63, and compared these metabolites to those found in cells infected by the mutant phage in which the two genes were deleted. These analyses revealed the presence of two unique molecules with *m/z* values of 720.010 and 622.034, respectively (in positive ionization mode). These molecules were exclusively observed when the cells were infected with the wild-type Bas63 in the presence of the SIR2–HerA defence system, but not in cells infected by the mutant

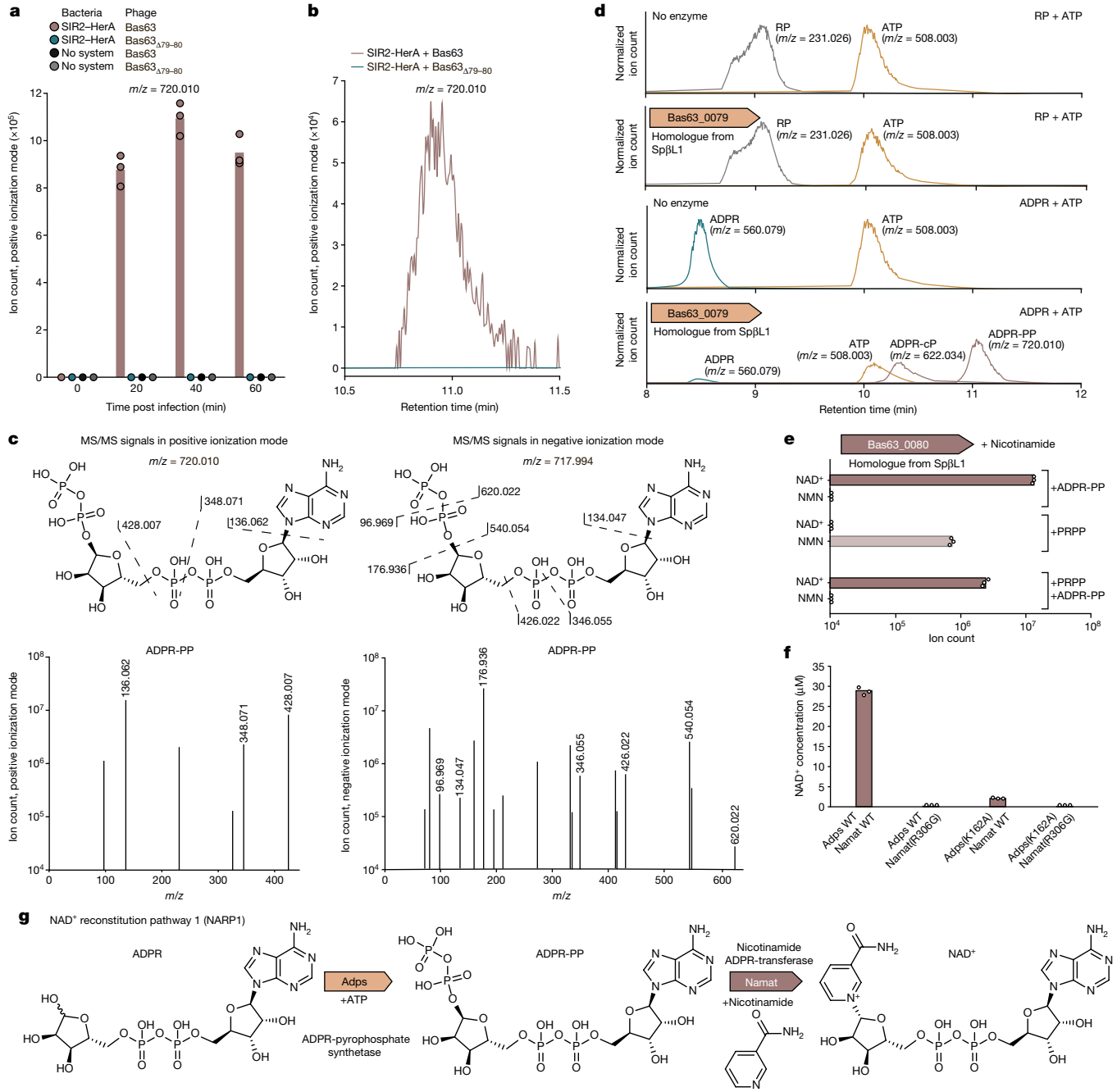

Fig. 2 | A two-enzyme pathway reconstitutes NAD$^+$ from ADPR and nicotinamide. a, A unique molecule with an *m/z* value of 720.010 appears in SIR2–HerA-expressing cells infected by Bas63. Cells were infected at MOI = 10. Presented are liquid chromatography (LC)–MS ion count data; bars represent the mean area under the curve of three experiments, with individual data points overlaid. **b**, Extracted mass chromatograms of ions with an *m/z* value of 720.010 (positive ionization mode) and retention time of 11.0 min, from a lysate of SIR2–HerA cells 20 min post infection by phage Bas63 or Bas63$_{\Delta 79–80}$. Chromatograms of the same molecule in negative ionization mode are presented in Extended Data Fig. 2c. **c**, MS/MS fragmentation spectra of the molecule with the *m/z* value of 720.010, in positive and negative ionization modes. The proposed structure of the molecule and the corresponding MS/MS fragments are presented. **d**, A homologue of the protein encoded by Bas63_0079 was purified from phage SpβL1 and incubated in the presence of ATP with either RP or ADPR. Shown are LC–MS analyses of the enzymatic reactions. Peak intensities of each compound were normalized to the signal of the corresponding standard sample (Methods). Representative chromatograms of three replicates are presented. **e**, A homologue of the protein encoded by Bas63_0080 was purified from phage SpβL1, and incubated with ADPR-PP, PRPP or a mixture of ADPR-PP and PRPP, in the presence of nicotinamide. Shown are data for the molecules NAD$^+$ and NMN measured through LC–MS. Bars represent the mean area under the curve of three experiments. **f**, Wild-type Adps and wild-type Namat, as well as active-site-mutated versions, were incubated with nicotinamide, ADPR and ATP. NAD$^+$ concentration was determined using the NAD/NADH-Glo assay. For **e**,**f**, bar graphs represent the average of three independent replicates with individual data points overlaid. **g**, Schematic of NARP1.

Bas63 phage (Fig. 2a,b and Extended Data Fig. 2a,b). The molecules were also not observed in control cells lacking the system that were infected by wild-type Bas63, suggesting that these unique molecules are formed only in the presence of the defence system, and only when the phage encodes the two anti-defence genes (Fig. 2a,b and Extended Data Fig. 2a,b). Tandem MS (MS/MS) analysis of the 720.010 molecule revealed fragments conforming with a pyrophosphorylated form of ADPR (ADPR-PP), a molecule that, to our knowledge, has not been

described previously in biological systems (Fig. 2c and Extended Data Fig. 2c). MS/MS analysis of the second mass suggested it to be ADPR cyclic phosphate (ADPR-cP), a likely product of spontaneous cyclization of ADPR-PP (Extended Data Fig. 2d).

The possible appearance of ADPR-PP in SIR2–HerA-expressing cells infected by Bas63 led us to reason that the phage gene annotated as *prs* (the first gene in the two-gene phage operon, Fig. 1a) does not encode a Prs enzyme, but rather an enzyme that pyro-phosphorylates ADPR. Under this hypothesis, instead of adding two phosphates to ribose 5-phosphate (RP) to generate PRPP, the phage enzyme would catalyse the addition of two phosphates to the ribose moiety of ADPR to generate ADPR-PP. PRPP is known to be easily cyclized to form 5-phosphorylribose 1,2-cyclic phosphate (PRcP)[20]. It is likely that the ADPR-PP analogue could also undergo similar spontaneous cyclization, leading to the formation of ADPR-cP and possibly explaining the appearance of the ion with the 622.034 *m*/*z* value (Extended Data Fig. 2a,b).

To further examine the enzymatic activity of the putative ADPR-PP-generating phage enzyme, we attempted to express and purify it for in vitro analyses. As the protein from Bas63 did not purify well, we instead used a homologous operon from phage SpβL1[21] from which we were able to obtain a purified protein (Extended Data Fig. 3a). Incubation of the purified protein with RP and ATP did not yield any measurable product, further supporting the hypothesis that this enzyme is not Prs (Fig. 2a). However, incubation of the protein with ADPR and ATP resulted in the formation of the same two molecules detected in our analysis of cellular metabolites during infection in vivo (Fig. 2d).

To establish the identity of the enzyme products, we treated the products of the enzymatic reaction with NudC, an enzyme of the NUDIX family that cleaves internal nucleoside-linked phosphate–phosphate bonds. As expected from the structure of ADPR-PP, incubation of the molecule suspected to be ADPR-PP with NudC resulted in the formation of PRPP, and similarly, NudC treatment of the molecule suspected to be ADPR-cP yielded PRcP as a product (Extended Data Fig. 4a). Treatment with apyrase, an enzyme that degrades terminal diphosphates into monophosphates, resulted in the formation of ADPR monophosphate from ADPR-PP (Extended Data Fig. 4b). Together, these results indicate that the purified phage enzyme probably catalyses the addition of pyrophosphate to ADPR in an ATP-dependent manner. To our knowledge, pyrophosphorylation of ADPR is an enzymatic reaction that has not been previously described. We named the phage enzyme ADPR-PP synthetase (Adps).

On the basis of its sequence annotation, the second protein encoded by the phage operon was expected to transfer a nicotinamide molecule to PRPP, replacing the high-energy pyrophosphate moiety with nicotinamide to generate NMN (Fig. 1b). Given that the first enzymatic reaction in this pathway generates ADPR-PP rather than PRPP, we reasoned that the second enzyme would use ADPR-PP as a substrate, and conjugate the nicotinamide instead of the pyrophosphate to directly generate NAD^+. To test this hypothesis, we expressed and purified this second enzyme encoded in the operon of phage SpβL1, and incubated the purified protein with ADPR-PP and nicotinamide. This resulted in the formation of NAD^+, confirming our hypothesis (Fig. 2e). To our knowledge, this reaction, too, has not been described previously in other biological systems. We named the second phage enzyme nicotinamide ADPR transferase (Namat). Both Namat and Adps have high affinity for their substrates, and the measured enzymatic catalytic constant, k_{cat}, values were similar to those of other enzymes involved in NAD^+ biosynthesis[22,23] (Extended Data Fig. 3b–e).

When incubated with PRPP and nicotinamide, the phage Namat enzyme was capable of producing NMN, but when exposed to a mixture of PRPP and ADPR-PP together with nicotinamide, only NAD^+ was detected as a product, suggesting a preference for this enzyme to use ADPR-PP as a substrate (Fig. 2e). Incubating a mixture of Adps and Namat with ADPR, nicotinamide and ATP resulted in the production of NAD^+ in vitro (Fig. 2f). The two-enzyme mixture was not able to efficiently produce NAD^+ if the predicted active site of Adps was impaired by substituting alanine for K162, or if the predicted active site of Namat was modified by a R306G substitution, further confirming that both enzymatic activities are essential for NAD^+ reconstitution (Fig. 2f). Together, our results reveal a phage-encoded two-step enzymatic pathway that can reconstitute NAD^+ from ADPR and nicotinamide in an ATP-dependent manner (Fig. 2g). We name this pathway NARP1.

NAD^+ synthesis overcomes defence systems

NAD^+-depleting defence systems that rely on SIR2, TIR or SEFIR domains cleave the glycosidic bond in NAD^+ to achieve NAD^+ depletion, producing the degradation products ADPR and nicotinamide[1–3]. Therefore, a pathway that can use these same products to rebuild NAD^+ would be an efficient solution for the phage to counter NAD^+ depletion by any of these defence systems. To test this hypothesis, we examined the effect of NARP1 on four additional defence systems: type I Thoeris, DSR1, DSR2 and SEFIR. Type I Thoeris is a two-gene system that encodes among its products an effector with a SIR2 domain, which was shown to deplete NAD^+ in response to phage infection[3]. DSR1 and DSR2 are large defensive proteins, each of which activates an amino-terminal SIR2 domain to deplete NAD^+ when a phage is detected by the carboxy-terminal domain of the protein[2]; and SEFIR is a single-protein defence system that depletes NAD^+ through its N-terminal SEFIR domain[1]. Co-expression of NARP1 in *Bacillus subtilis* with any of these systems abolished the system's ability to defend against *Bacillus* phages, confirming the generality of NARP1 in countering multiple defence systems (Fig. 3a). Point mutation affecting the active sites of either of the two proteins in NARP1 impaired its ability to efficiently counter defence (Fig. 3a).

As a control for these experiments, we used type II Thoeris, a defence system that functions similarly to type I Thoeris, but in which the SIR2 domain is replaced by two transmembrane helices that are thought to induce membrane permeability when the system detects phage infection, causing premature cell death independent of NAD^+ (ref. 24). Expression of NARP1 with type II Thoeris did not abolish defence, further supporting the assumption that NARP1 can counter only bacterial defences that rely on NAD^+ depletion (Fig. 3b).

NAD^+ synthesis pathway is phage-specific

Given the homology between the phage enzyme Adps and the bacterial Prs enzyme, we sought to study the evolutionary relationship between the two enzymes and their taxonomic distribution across the phylogenetic tree. For this, we searched a database of about 4,000 finished bacterial and archaeal genomes[1] and a database of about 20,000 complete phage genomes[25] for homologues of Prs and Adps. A phylogenetic analysis of the detected homologues revealed that Adps proteins localize to a well-supported clade that is separated from most prokaryotic Prs homologues, and that appears almost exclusively in phage genomes (Fig. 3c). In a minority of cases, sequences in the Adps clade were present in bacterial genomes, and in some, but not all, of these cases, Adps was within prophages or other mobile genetic elements integrated in the bacterial genome (see Discussion and Supplementary Table 1).

We next examined the genomic neighbourhood of genes encoding Prs and Adps homologues. For most proteins in the Adps clade (97%), we detected a homologue of Namat in the immediate vicinity of the *adps* gene, confirming the functional association between Adps and Namat in NARP1 (Fig. 3c). By contrast, bacterial *prs* genes were only very rarely present next to a gene encoding a Namat homologue. Altogether, our analyses suggest that Adps proteins form a subfamily within the Prs family of proteins, and that such Adps proteins evolved to utilize ADPR as a substrate instead of RP as part of NARP1.

We detected NARP1 encoding Adps and Namat in 859 sequenced phage genomes, representing 4.3% of the phages in the set we

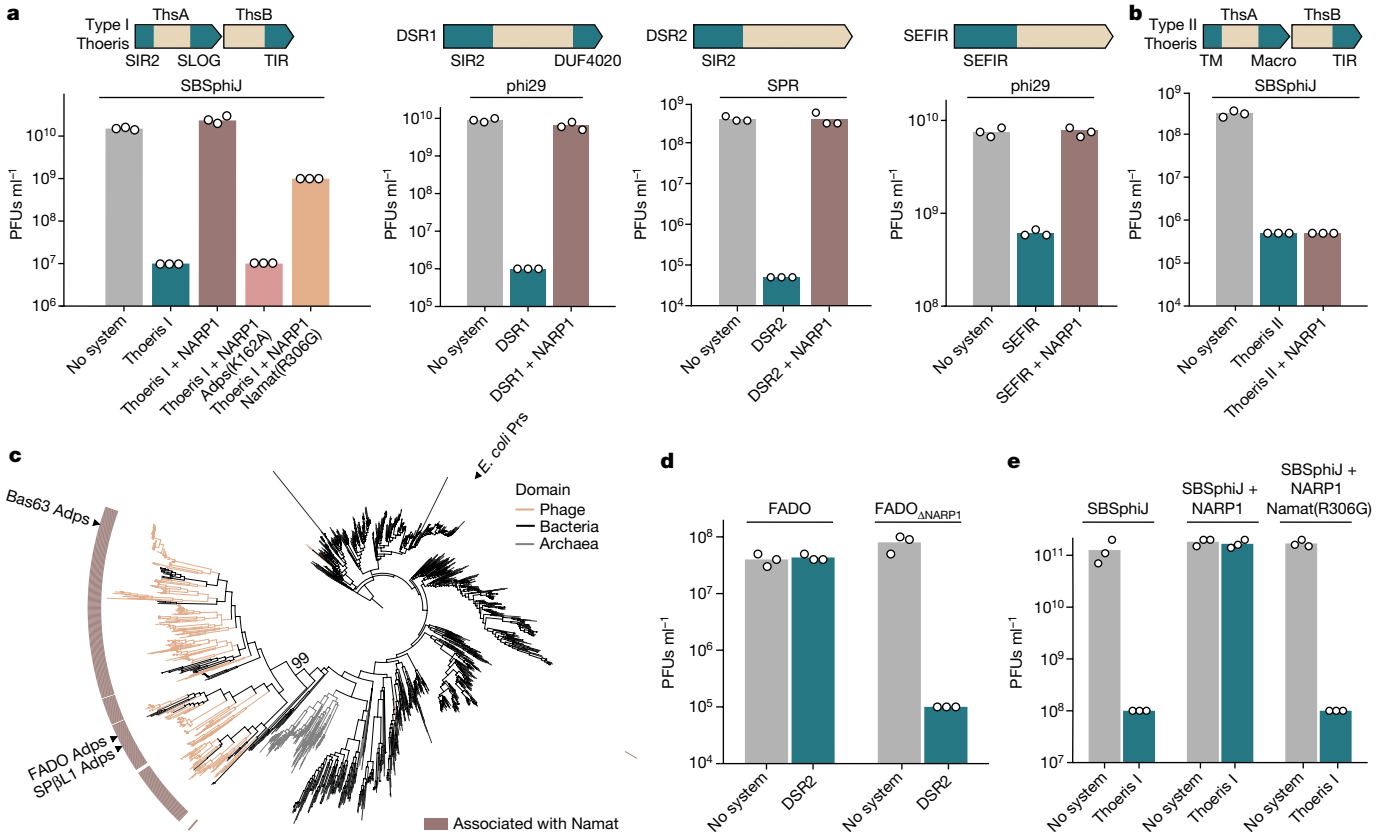

Fig. 3 | NARP1 is a phage-specific pathway that overcomes multiple NAD$^+$ depletion defence systems. a, Anti-defence effect of NARP1 co-expressed in *B. subtilis* together with diverse NAD$^+$-depleting defence systems. Data represent PFUs per millilitre of *Bacillus* phages infecting control cells (no system), cells expressing the respective defence systems and cells co-expressing the defence system and NARP1. For type I Thoeris, results for co-expression of mutated versions of NARP1 are also presented. **b**, NARP1 does not overcome type II Thoeris, a defence system that does not deplete NAD$^+$ as part of its mechanism. Data presented are as in **a**. **c**, Phylogenetic analysis of the Adps and Prs protein family in phages, bacteria and archaea. Genes were marked as associated with Namat if a Namat homologue was detected in the genomic vicinity (up to ten genes from the Prs- or Adps-encoding gene). Prokaryotic and viral protein sequences were clustered separately on the basis of identical length and >90% identity, and a representative sequence of each cluster was used to build the tree (Methods). Ultrafast bootstrap value[37] is shown for the Adps clade. **d**, Deletion of the NARP1 operon sensitizes the FADO phage to the DSR2 defence system. Data represent PFUs per millilitre of FADO and FADO$_{\Delta NARP1}$ phages infecting control cells (no system) and cells expressing the DSR2 defence system. **e**, Knock-in of the NARP1 operon into phage SBSphiJ makes it resistant to type I Thoeris defence. Data represent PFUs per millilitre of wild-type SBSphiJ, SBSphiJ with NARP1 operon knock-in and SBSphiJ with the NARP1 operon with an active site alteration encoded in knocked-in Namat. Phages were used to infect control cells (no system) and cells expressing type I Thoeris. In **a**,**b**,**d**,**e**, bar graphs represent the average of three independent replicates, with individual data points overlaid. In each panel, phages that were used are indicated above the respective bar graphs.

analysed (Supplementary Table 1). To assess the generality of our findings, we questioned whether additional homologues of this NAD$^+$ reconstitution pathway also endow phages with the ability to evade NAD$^+$-depletion-mediated defence. For this, we examined NARP1 from phage FADO, a lytic phage that we previously isolated[1], and generated a mutant of FADO in which the two genes encoding NARP1 were deleted. The mutant phage could not replicate in cells expressing the defence system DSR2, whereas the wild-type FADO phage overcame defence (Fig. 3d). To further test whether NARP1 can protect phages from the effects of NAD$^+$ depletion independently of other phage factors, we engineered NARP1 from SpβL1 into phage SBSphiJ, a phage that is naturally sensitive to the type I Thoeris defence system. We found that the engineered phage can overcome the type I Thoeris system (Fig. 3e), whereas a phage engineered with mutated NARP1 could not overcome Thoeris defence. Our data confirm the broad function of the viral NARP1 in counteracting NAD$^+$-depletion-based bacterial defences.

A second NAD$^+$ synthesis pathway in phages

We next searched for homologues of the NARP1 Namat proteins in the set of about 20,000 phage genomes. Although most (about 79%) Namat proteins were found in phages that also encode Adps, we observed that about 20% of homologues were encoded in phages that lack any homologue of Adps. A phylogenetic analysis showed that these homologues organize into a clade distinct from the clade encoding the NARP1-associated Namat proteins, suggesting that this clade encodes proteins that have sequence homology to NARP1 Namat enzymes but may have a different enzymatic function (Fig. 4a and Supplementary Table 2).

One of the proteins in the new clade is encoded in *Vibrio* phage KVP40 (Fig. 4a,b). This protein was previously shown to have a Nampt activity, capable of producing NMN from PRPP and nicotinamide[26]. To test whether this protein is also capable of producing NAD$^+$ from ADPR-PP, we purified the protein and incubated it with either PRPP, ADPR-PP or both PRPP and ADPR-PP, all in the presence of nicotinamide and ATP. Our data reproduced the previous observation that the protein has Nampt enzymatic activity[26]. Although we could observe the production of NAD$^+$ from ADPR-PP, a reaction in which both ADPR-PP and PRPP were supplied as substrates to the purified protein showed that this enzyme prefers PRPP as a substrate (Fig. 4c).

It was previously shown that a second gene in *Vibrio* phage KVP40 encodes an NMN adenylyltransferase (Nmnat), capable of generating

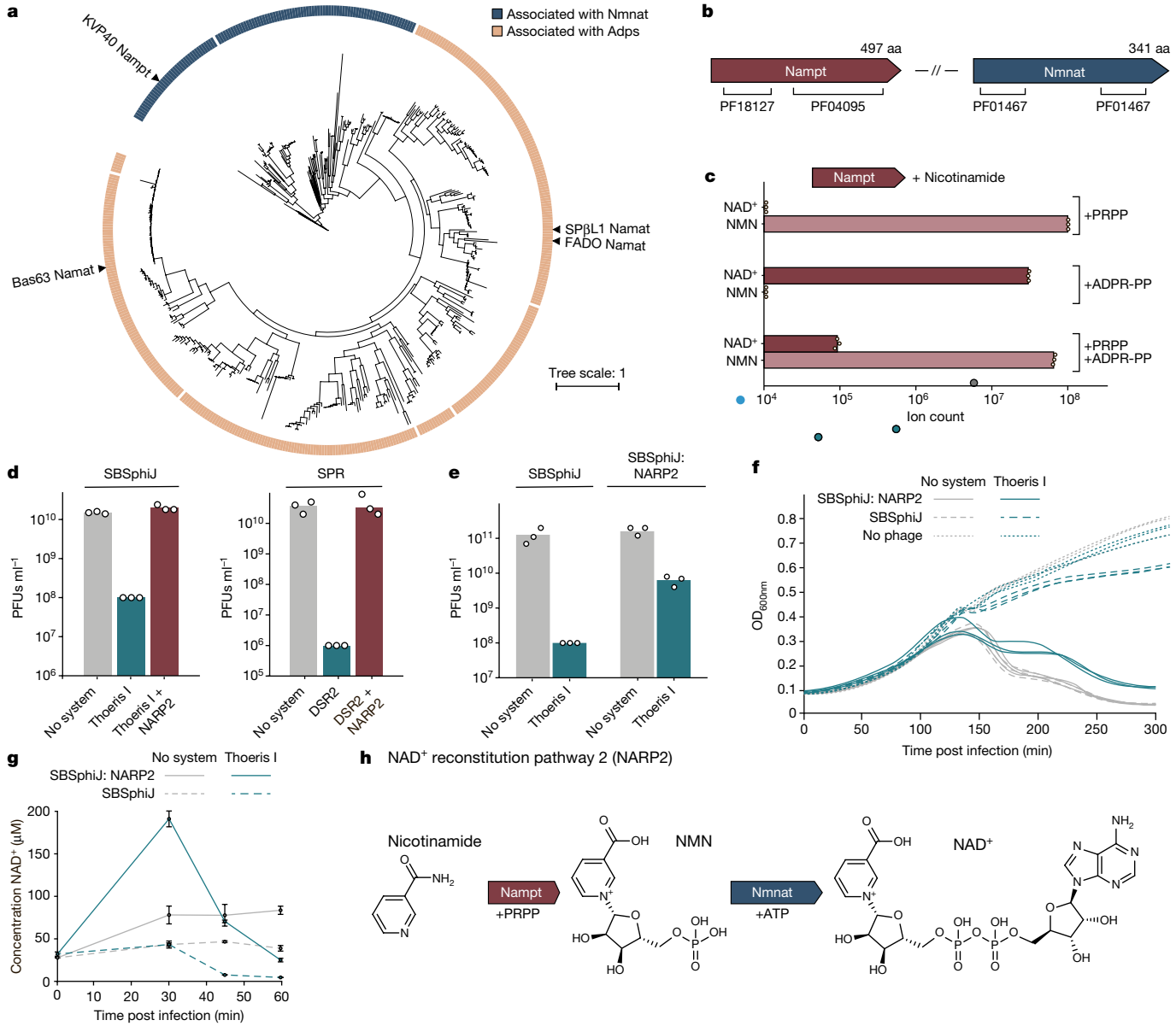

Fig. 4 | NARP2 is a second NAD$^+$ reconstitution pathway allowing phages to overcome bacterial defence. a, Phylogenetic analysis of the Namat and Nampt protein family in phage genomes. The outer ring indicates whether the phage also encodes Nmnat (blue) or whether the gene is associated with Adps (beige) as defined in Fig. 3c. **b**, Domain annotations of the NAD$^+$ salvage proteins from *Vibrio* phage KVP40. **c**, Purified Nampt from *Vibrio* phage KVP40 was incubated with PRPP, ADPR-PP or a mixture of ADPR-PP and PRPP, in all cases in the presence of nicotinamide. The products NAD$^+$ and NMN were measured by LC–MS. Data represent the mean area under the curve of three experiments. **d**, NARP2, when co-expressed with NAD$^+$-depleting defence systems, inhibits antiphage defence. Data represent PFUs per millilitre of phages infecting control cells (no system), cells expressing the indicated defence systems and cells co-expressing the defence system and NARP2. **e**, Knock-in of the NARP2 operon into phage SBSphiJ results in partial resistance to type I Thoeris defence. Data represent PFUs per millilitre of phages SBSphiJ and SBSphiJ+NARP2 infecting control cells (no system) and cells expressing type I Thoeris. Phages used for the infection assays are indicated above the graph. **f**, Liquid culture growth of *B. subtilis* cells expressing type I Thoeris, or control cells without defence genes (no system). Cells were infected by phages SBSphiJ and SBSphiJ with the NARP2 operon knocked in. Infection was carried out at MOI = 0.1. Data from three replicates are presented as individual curves. **g**, NAD$^+$ concentration in lysates extracted from cells expressing type I Thoeris or control strain (no system). Cells were infected with either phage SBSphiJ or SBSphiJ with the NARP2 operon knocked in, at MOI = 10. Cells were collected before infection (0 min) and 30, 45 or 60 min after infection. Data are presented as mean values ± s.d., $n = 3$ replicates. **h**, Schematic of the enzymatic reactions of NARP2[26]. For **b**,**d**,**e**, bar graphs represent the average of three independent replicates with individual data points overlaid.

NAD$^+$ by conjugating AMP to NMN[26] (Fig. 4a). Moreover, it was shown that the *Vibrio* phage KVP40 Nmnat, together with the Nampt from the same phage, can generate NAD$^+$ from RP, nicotinamide and ATP[26]. Given that these two proteins represent an NAD$^+$ reconstitution pathway that functions through enzymatic reactions different from those encoded by NARP1, we reasoned that the KVP40 pathway, too, can save phages from the effects of NAD$^+$-depleting defence systems.

To test this hypothesis, we co-expressed these two genes in cells expressing either type I Thoeris or DSR2, and infected these cells with phages known to be blocked by the respective defence systems. Our data show that the two genes from KVP40 completely abolished the activity of both Thoeris and DSR2 (Fig. 4d). We next integrated these two genes from phage KVP40 into the genome of phage SBSphiJ, which is naturally blocked by type I Thoeris, and found

that the engineered phage was able to overcome Thoeris defence (Fig. 4e,f).

To further examine whether the two genes supply the phage with NAD^+ despite the activity of the defence system, we measured NAD^+ levels during infection, and detected a substantial increase in NAD^+ levels in cells infected by the SBSphiJ phage engineered to express the two genes from KVP40 (Fig. 4g). The increase of NAD^+ levels was also observed in SBSphiJ-infected *B. subtilis* cells that did not encode the defence system, suggesting that this pathway generates NAD^+ regardless of the activity of NAD^+-depleting defence systems (Fig. 4g), corroborating previous reports on the *Vibrio* KVP40 phage that naturally encodes these genes[26].

Our data show that almost all phages (94%) in which we detected a homologue of the KVP40 Nampt enzyme also encode a homologue of Nmnat, providing further support that these two proteins are functionally linked and form an NAD^+ reconstitution pathway (Fig. 4h and Supplementary Table 2). Our data suggest that the function of this pathway is to counter the activity of NAD^+-depleting defence systems. We name this pathway NAD^+ reconstitution pathway 2 (NARP2), and find that NARP2 is encoded in about 1.1% of sequenced phage genomes (Supplementary Table 2). We were not able to find any phage that encodes both NARP1 and NARP2 (Supplementary Table 2).

Discussion

Phages are known to encode multiple proteins to counter bacterial defences[21,27,28]. In most cases, each anti-defence phage protein inhibits only a narrow range of defence systems. Most anti-CRISPR proteins, for example, bind and inhibit only a specific subtype of CRISPR–Cas[29], and Apyc1, a phage protein that degrades immune signalling molecules, inhibits only the Pycsar system[30]. The phage anti-defence strategy we describe in the current study is unique because it counters the consequences of the immune action rather than components of the defence system itself. Thus, it allows phages to evade a wide variety of systems that deplete NAD^+, including SIR2–HerA[2], DSR1[2], DSR2[2] and type I Thoeris[3], and is likely to also overcome variants of CBASS[6], Pycsar[7], AVAST[5] and pAgo[2,4] that have effectors that deplete NAD^+.

Although both NARP1 and NARP2 rebuild NAD^+ as their final products, they differ in their substrates. NARP1 uses ADPR and nicotinamide, the direct products of NAD^+ cleavage by immune effector domains such as TIR, SIR2 and SEFIR[1–3], and necessitates only ATP in addition to the cleavage products for the production of NAD^+. This pathway will therefore not come into action unless the phage infects a cell that contains an NAD^+-depleting system, and unless the system actively depletes NAD^+ in an attempt to protect against the infecting phage. As ADPR is normally not present in substantial quantities in uninfected *B. subtilis* cells[2], this pathway probably inflicts minimal metabolic costs to the phage when infecting cells that do not encode an NAD^+-depleting defence system. Indeed, we did not observe production of excessive NAD^+ when NARP1-containing phages infected cells that lack a defence system (Fig. 1e). By contrast, phages encoding NARP2 caused cells to produce excessive NAD^+ during infection even when the cells did not contain an NAD^+-depleting defence system, because NARP2 uses PRPP as its starting substrate (Fig. 4g). Thus, NARP2 may inflict a greater metabolic cost to the phage, especially as it consumes PRPP, which is essential for nucleotide synthesis[23]. The possibly higher metabolic cost inflicted by NARP2 may explain why it is rarer in phage genomes as compared to NARP1.

As at least 7% of all bacteria whose genomes were sequenced encode an NAD^+-depleting defence system[1], it is not unexpected that NARP1 and NARP2 together are present in 5.4% of sequenced phages. A recent analysis of phage genomes shows that in addition to NARP1 and NARP2, phages can encode other genes whose annotations suggest involvement in NAD^+ salvage[15]. For example, some phages encode homologues of NadR, an enzyme known to produce NAD^+ from nicotinamide riboside and ATP[15]. Phage NadR-encoding genes are usually present in the same operon as a gene annotated as encoding PnuC, a transporter specific for nicotinamide riboside, and it is conceivable that this operon would form yet another pathway allowing phages to produce NAD^+ through available metabolites (Extended Data Fig. 1b). Thus, the actual fraction of phages encoding an NAD^+ reconstitution pathway may be even larger than the >5% we recorded.

Although NARP1 is preferentially encoded in phages, some bacterial genomes seem to encode it not in the context of a prophage or a mobile genetic element (Supplementary Table 1). ADPR was shown, in a minority of bacteria, to be present at detectable concentrations[31], and it was demonstrated that this metabolite may be involved in regulation of transcription in some bacteria[32]. It is therefore possible that some bacteria have adopted NARP1 for housekeeping or regulatory functions not related to the phage-bacteria conflict; future studies will be necessary to determine the role of NARP1 in this context.

In recent years, multiple bacterial immune systems were shown to degrade essential metabolites as a measure of antiphage defence, representing a general strategy of depriving the phage of an essential metabolite and limiting its propagation. In addition to NAD^+ depletion, metabolite-depleting defence systems include dCTP deaminases[33] and dGTPases[33] that degrade deoxynucleotides, and ATP nucleosidases that deplete ATP in infected cells[13]. It is possible that, similar to NAD^+ reconstitution pathways, phages may also encode pathways that rebuild deoxynucleotides or ATP from the degradation products generated by the respective defence system. As depletion of deoxynucleotides and ATP is utilized by animal cells as an antiviral measure[13,34], and moreover as NAD^+ is known to participate in the conflict between animal cells and viruses[35,36], future studies may reveal that viruses infecting animals may also use metabolite reconstitution as a counter-defence strategy.

Online content

Any methods, additional references, Nature Portfolio reporting summaries, source data, extended data, supplementary information, acknowledgements, peer review information; details of author contributions and competing interests; and statements of data and code availability are available at https://doi.org/10.1038/s41586-024-07986-w.

1. Millman, A. et al. An expanded arsenal of immune systems that protect bacteria from phages. *Cell Host Microbe* **30**, 1556–1569 (2022).
2. Garb, J. et al. Multiple phage resistance systems inhibit infection via SIR2-dependent NAD^+ depletion. *Nat. Microbiol.* **7**, 1849–1856 (2022).
3. Ofir, G. et al. Antiviral activity of bacterial TIR domains via immune signalling molecules. *Nature* **600**, 116–120 (2021).
4. Zaremba, M. et al. Short prokaryotic Argonautes provide defence against incoming mobile genetic elements through NAD^+ depletion. *Nat. Microbiol.* **7**, 1857–1869 (2022).
5. Gao, L. A. et al. Prokaryotic innate immunity through pattern recognition of conserved viral proteins. *Science* **377**, eabm4096 (2022).
6. Morehouse, B. R. et al. STING cyclic dinucleotide sensing originated in bacteria. *Nature* **586**, 429–433 (2020).
7. Tal, N. et al. Cyclic CMP and cyclic UMP mediate bacterial immunity against phages. *Cell* **184**, 5728–5739 (2021).
8. Chen, Y. et al. From bacteria to biomedicine: developing therapies exploiting NAD^+ metabolism. *Bioorg. Chem.* **142**, 106974 (2024).
9. Erhardt, H. et al. Organization of the *Escherichia coli* aerobic enzyme complexes of oxidative phosphorylation in dynamic domains within the cytoplasmic membrane. *MicrobiologyOpen* **3**, 316–326 (2014).
10. Rodionova, I. A. et al. Metabolic and bactericidal effects of targeted suppression of NadD and NadE enzymes in mycobacteria. *mBio* **5**, e00747-13 (2014).
11. Mikolcevic, P., Hlousek-Kasun, A., Ahel, I. & Mikoc, A. ADP-ribosylation systems in bacteria and viruses. *Comput. Struct. Biotechnol. J.* **19**, 2366–2383 (2021).
12. Wilkinson, A., Day, J. & Bowater, R. Bacterial DNA ligases. *Mol. Microbiol.* **40**, 1241–1248 (2001).
13. Rousset, F. et al. A conserved family of immune effectors cleaves cellular ATP upon viral infection. *Cell* **186**, 3619–3631 (2023).
14. Maffei, E. et al. Systematic exploration of *Escherichia coli* phage-host interactions with the BASEL phage collection. *PLoS Biol.* **19**, e3001424 (2021).
15. Iyer, L. M., Burroughs, A. M., Anantharaman, V. & Aravind, L. Apprehending the NAD^+–ADPr-dependent systems in the virus world. *Viruses* **14**, 1977 (2022).
16. Gazzaniga, F., Stebbins, R., Chang, S. Z., McPeek, M. A. & Brenner, C. Microbial NAD metabolism: lessons from comparative genomics. *Microbiol. Mol. Biol. Rev.* **73**, 529–541 (2009).

17. Tang, D. et al. Multiple enzymatic activities of a Sir2-HerA system cooperate for anti-phage defense. *Mol. Cell* **83**, 4600–4613 (2023).
18. Galeazzi, L. et al. Identification of nicotinamide mononucleotide deamidase of the bacterial pyridine nucleotide cycle reveals a novel broadly conserved amidohydrolase family. *J. Biol. Chem.* **286**, 40365–40375 (2011).
19. Raffaelli, N. et al. The *Escherichia coli* NadR regulator is endowed with nicotinamide mononucleotide adenylyltransferase activity. *J. Bacteriol.* **181**, 5509–5511 (1999).
20. Khorana, H. G., Fernandes, J. F. & Kornberg, A. Pyrophosphorylation of ribose 5-phosphate in the enzymatic synthesis of 5-phosphorylribose 1-pyrophosphate. *J. Biol. Chem.* **230**, 941–948 (1958).
21. Yirmiya, E. et al. Phages overcome bacterial immunity via diverse anti-defence proteins. *Nature* **625**, 352–359 (2024).
22. Revollo, J. R., Grimm, A. A. & Imai, S. The NAD biosynthesis pathway mediated by nicotinamide phosphoribosyltransferase regulates Sir2 activity in mammalian cells. *J. Biol. Chem.* **279**, 50754–50763 (2004).
23. Hove-Jensen, B. et al. Phosphoribosyl diphosphate (PRPP): biosynthesis, enzymology, utilization, and metabolic significance. *Microbiol Mol Biol Rev* **81**, e00040-16 (2017).
24. Sabonis, D. et al. TIR domains produce histidine-ADPR conjugates as immune signaling molecules in bacteria. Preprint at *bioRxiv* https://www.biorxiv.org/content/10.1101/2024.01.03.573942v1 (2024).
25. Cook, R. et al. INfrastructure for a PHAge REference Database: identification of large-scale biases in the current collection of cultured phage genomes. *Phage* **2**, 214–223 (2021).
26. Lee, J. Y., Li, Z. & Miller, E. S. *Vibrio* phage KVP40 encodes a functional NAD^+ salvage pathway. *J. Bacteriol.* **199**, e00855-16 (2017).
27. Gao, Z. & Feng, Y. Bacteriophage strategies for overcoming host antiviral immunity. *Front. Microbiol.* **14**, 1211793 (2023).
28. Mayo-Munoz, D., Pinilla-Redondo, R., Camara-Wilpert, S., Birkholz, N. & Fineran, P. C. Inhibitors of bacterial immune systems: discovery, mechanisms and applications. *Nat. Rev. Genet.* **25**, 237–254 (2024).
29. Zhang, F., Song, G. & Tian, Y. Anti-CRISPRs: the natural inhibitors for CRISPR-Cas systems. *Animal Model. Exp. Med.* **2**, 69–75 (2019).
30. Hobbs, S. J. et al. Phage anti-CBASS and anti-Pycsar nucleases subvert bacterial immunity. *Nature* **605**, 522–526 (2022).
31. Huang, N. et al. Structure and function of an ADP-ribose-dependent transcriptional regulator of NAD metabolism. *Structure* **17**, 939–951 (2009).
32. Rodionov, D. A. et al. Transcriptional regulation of NAD metabolism in bacteria: NrtR family of Nudix-related regulators. *Nucleic Acids Res.* **36**, 2047–2059 (2008).
33. Tal, N. et al. Bacteria deplete deoxynucleotides to defend against bacteriophage infection. *Nat. Microbiol.* **7**, 1200–1209 (2022).
34. Goldstone, D. C. et al. HIV-1 restriction factor SAMHD1 is a deoxynucleoside triphosphate triphosphohydrolase. *Nature* **480**, 379–382 (2011).
35. Heer, C. D. et al. Coronavirus infection and PARP expression dysregulate the NAD metabolome: an actionable component of innate immunity. *J. Biol. Chem.* **295**, 17986–17996 (2020).
36. Brenner, C. Viral infection as an NAD^+ battlefield. *Nat. Metab.* **4**, 2–3 (2022).
37. Minh, B. Q., Nguyen, M. A. & von Haeseler, A. Ultrafast approximation for phylogenetic bootstrap. *Mol. Biol. Evol.* **30**, 1188–1195 (2013).

Methods

Strains and growth conditions

E. coli K-12 BW25113, DH5a and BL21 (DE3) were grown in MMB medium (lysogeny broth (LB) supplemented with 0.1 mM $MnCl_2$ and 5 mM $MgCl_2$) at 37 °C with 200 r.p.m. shaking or on solid 1.5% LB agar plates. Ampicillin 100 μg ml^{-1}, chloramphenicol 30 μg ml^{-1} or kanamycin 50 μg ml^{-1} were added when necessary for plasmid maintenance. *E. coli* DH5a (NEB) was used for cloning, BL21 (DE3) was used for protein purification, and BW25113 was used for experiments with phages. *B. subtilis* strain BEST7003 (obtained from M. Itaya, Keio University, Japan) was grown in MMB at 25 °C or 30 °C; spectinomycin 100 μg ml^{-1} and/or chloramphenicol 5 μg ml^{-1} was added when needed. All chemicals were obtained from Sigma Aldrich unless stated otherwise. All phages used in the study were amplified from a single plaque at 37 °C (except for FADO, which was amplified at 25 °C) in *B. subtilis* BEST7003 culture in MMB until the culture collapsed. A list of all plasmids, strains and phages used in this study can be found in Supplementary Table 3.

Plasmid construction and transformation

DNA amplification for cloning was carried out using KAPA HiFi HotStart ReadyMix (Roche) according to the manufacturer's instructions. All primers were obtained from Sigma Aldrich. Supplementary Table 4 lists all primers used in this study.

For site-directed mutagenesis, the whole plasmid was amplified by back-to-back primers containing mutations at the primer 5′-end. PCR product was then directly used for circularization with KLD enzyme mix (NEB) according to the manufacturer's instructions, and used for transformation. For cloning of large fragments, PCR products with 20-nucleotide overlaps were generated and treated with FastDigest DpnI (ThermoFisher) restriction enzyme for 30 min at 37 °C. Fragments were then Gibson assembled using NEBuilder HiFi DNA Assembly Master Mix (NEB) according to the manufacturer's instructions and used for transformation into DH5a (NEB number C2987H). Single colonies were checked by PCR and plasmids were validated by a plasmid sequencing service (Plasmidsaurus).

Verified plasmids were transformed into *E. coli* using the standard transformation and storage solution protocol[38] or to *B. subtilis* using MC medium as previously described[39]. The KVP40 NARP2 operon (Supplementary Table 3) could not be transformed into *E. coli* because of toxicity, and hence the Gibson assembly product was directly transformed into *B. subtilis* using the MC medium protocol. Integrations of the NARP1 and NARP2 constructs into *B. subtilis* strains were confirmed by whole-genome sequencing.

To design active site alterations of Adps and Namat, we aligned their sequences with previously studied homologues. SpβL1 Adps is similar to *B. subtilis* Prs (27% sequence identity), in which Lys197 was previously demonstrated biochemically and structurally to be essential for the enzymatic activity[40,41]. Therefore, Lys162 of Adps from SpβL1, corresponding to Lys197 of *B. subtilis* Prs, was substituted to alanine by site-directed mutagenesis. SpβL1 Namat shares 33% sequence identity with the *Homo sapiens* NAMPT protein, the active site of which was studied biochemically and structurally[40]. An Arg306-to-glycine substitution was designed in the SpβL1 Namat on the basis of the homologous residue Arg311 shown to be important for the activity of the human NAMPT[40]. Primers for site-directed mutagenesis of both genes are listed in Supplementary Table 4.

Deletion of NARP1 operons from Bas63 and FADO phages

The NARP1 operon from Bas63 was deleted using Cas13a as previously described[42]. A guide RNA (gRNA) complementary to the beginning of the coding region of gene 79 was cloned into the plasmid pBA559 treated with BsaI. *E. coli* DH5a was transformed with this plasmid and then infected by Bas63 in two consecutive rounds with MOI ≈ 1 in 5 ml of MMB medium. Then, 100 μl of lysate was spread on a plate with the same strain (DH5a without plasmid was used as a control). Several plaques were collected and screened by PCR. Deletion of the genomic region starting from codon 28 of gene 79 and ending in coding 302 of gene 80 was confirmed by whole-genome sequencing of the phage genome.

To delete the NARP1 region from the FADO phage, lysogenic bacteria were first prepared by infecting *B. subtilis* strain BEST7003 cells with the FADO phage (MOI 0.1). When cells started to grow again after lysis, the culture was spread onto an MMB-agar plate. Individual clones were selected and checked for lysogeny by incubation with mitomycin C (0.5 μg ml^{-1}) followed by phage titre counting in the supernatant. Lysogenic bacteria were transformed with a non-replicating *B. subtilis* plasmid (pJmp3) encoding a spectinomycin resistance gene flanked by 1-kilobase regions identical to the DNA flanking the NARP1 operon in the FADO genome. Following homologous recombination, spectinomycin-resistant lysogens were selected on a plate with spectinomycin and checked by PCR. The modified FADO prophage was induced using mitomycin C (0.5 μg ml^{-1}). Whole-genome sequencing was carried out to verify the sequence of the modified phage.

Knock-in of intact and mutated NARP1 and NARP2 operons into SBSphiJ

Insertion of DNA into the SBSphiJ genome was previously demonstrated to be achievable through homologous recombination[43]. Here we used the same region in the SBSphiJ genome previously used to knock-in the gene *tad1*[43], and the same flanking regions, to integrate the NARP1 and NARP2 operons into the SBSphiJ genome. Plasmids with intact and mutated NARP1 operons and Gibson assembly product for the NARP2 operon, flanked by 1-kilobase regions identical to the DNA flanking *tad1* in the SBSphiJ7 genome, were transformed into *B. subtilis* BEST7003 and these strains were infected by SBSphiJ with an MOI of 0.1 for generating recombined phages. A gRNA complementary to unmodified SBSphiJ was cloned into the previously published plasmid pGad2-Cas13a[21] to generate pCas13a-gRNA-SBSphiJ. *B. subtilis* BEST7003, transformed with this plasmid was used for selection against unmodified SBSphiJ phages to retain only phages in which homology recombination took place. The selection was made on an agar plate in the presence of 0.2% xylose, and several plaques were tested by PCR for the presence of intact and mutated NARP1 and NARP2. Whole-genome sequencing was carried out to verify the sequence of the modified phage.

Generation of Δ*pncC*Δ*nadR E. coli* strain by P1 transduction

The BW25113 Δ*nadR* strain from the Keio collection[44] was transformed with the pCP20 plasmid to eliminate the resistance cassette[44]. Kanamycin-sensitive clones were selected and checked by PCR. BW25113 Δ*pncC* from the Keio collection was infected with P1 and used as a donor for transduction, which was carried out according to the standard protocol[45]. Double knockouts were selected on kanamycin and checked by PCR; positive clones were grown for two passages on LB medium with 5 mM sodium citrate to eliminate the residual phage. The sequence of the Δ*pncC*Δ*nadR E. coli* was validated by a genome sequencing service (Plasmidsaurus).

Plaque assays

Phage titre was determined as described previously[46]. A 300 μl volume of the overnight bacterial cultures was mixed with 30 ml of melted MMB 0.5% agar, poured on 10-cm square plates and left to dry for 1 h at room temperature. Isopropyl-β-D-thiogalactoside was added to a concentration of 1 mM to induce NARP1 and NARP2 from the *B. subtilis* genome. Tenfold dilutions of phages were prepared in MMB and 10 μl of each dilution was dropped onto the plates. Plates were incubated overnight at 25 °C (DSR1, DSR2, SEFIR and type II Thoeris), 30 °C (type I Thoeris) and 37 °C (SIR2–HerA). PFUs were counted the next day.

Liquid infection assays

Overnight bacterial cultures were diluted in MMB and grown until reaching an OD_{600nm} of 0.3. Then, 180 µl of the cultures was transferred to a 96-well plate and infected with 20 µl of phages at various MOIs. Culture growth was followed by OD_{600nm} measurements every 10 min on a Tecan Infinite 200 plate reader. Cells expressing the SIR2–HerA system were grown at 37 °C, whereas those expressing the type I Thoeris system were grown at 30 °C.

Cell lysates preparation

E. coli BW25113 cells carrying a plasmid with the SIR2–HerA system or an empty plasmid were grown at 37 °C, 200 r.p.m., until reaching an OD_{600nm} of 0.3 in 250 ml of MMB. Cells were then infected with Bas63 and $Bas63_{\Delta 79-80}$ with MOI = 10. Samples were collected before infection and 20, 40 and 60 min after infection. At each time point, 50 ml of cells was centrifuged for 10 min at 25 °C, 4,000*g*, for 10 min to pellet the cells and 600 µl of 50% methanol/50% 0.1 M Na-phosphate buffer, pH 8.0, was immediately added to stop further NAD^+ degradation. Resuspended cells were frozen in liquid nitrogen and stored at −80 °C. To extract metabolites, resuspended cells were transferred to FastPrep Lysing Matrix B in a 2-ml tube (MP Biomedicals, number 116911100) and lysis was achieved as described previously[43]. Lysates were analysed by LC–MS or with the NAD/NADH-Glo kit (Promega). *B. subtilis* strain BEST7003 expressing type I Thoeris or a control strain without a defence system was grown at 30 °C, 200 r.p.m., until reaching an OD_{600nm} of 0.3 in 250 ml of MMB and then infected with SBSphiJ and SBSphiJ + NARP2 with MOI = 10. Samples were collected before infection and 30, 45 and 60 min after infection. The subsequent processing steps were carried out exactly as described above for the *E. coli* samples.

Protein purification

Plasmids were transformed into BL21 (DE3) cells, and cells were grown in MMB medium at 37 °C until mid-log phase ($OD_{600nm} \approx 0.5$); then isopropyl-β-D-thiogalactoside was added to a concentration of 0.5 mM and cells were further grown for another 3 h, centrifuged and flash-frozen. His-tagged proteins were purified by NEBExpress Ni-NTA Magnetic Beads (NEB) according to the manufacturer's protocol. Proteins were transferred to 20 mM Tris (pH 8), 200 mM NaCl, 5 mM dithiothreitol and 5% (v/v) glycerol by five cycles of filtration through 10-kDa Amicon filters (Merck Millipore), and finally concentrated to 0.5 mg ml^{-1}.

Enzymatic activity of purified proteins

End-point reactions (Figs. 2d–f and 4c) were carried out in 50 mM Tris (pH 7.5), 12 mM $MgCl_2$ and BSA 0.02% (w/v), and D-RP (Sigma 83875), 5-phospho-D-ribose 1-diphosphate (Sigma P8296), adenosine 5′-diphosphoribose (Sigma A0752) and nicotinamide were added to 1 mM when indicated. ATP was added in excess to a concentration of 5 mM in all reactions, except for that in Fig. 2d, in which ATP concentrations were 1 mM (equimolar). Adps was added at 0.5 µM; Namat and Nampt were added at 0.2 µM in all reactions. Reactions were incubated for 60 min at 30 °C and then stopped by adding methanol 50% and diluting 10 times in 50% methanol/50% 0.1 M Na-phosphate buffer, pH 8.0. Products and substrate molecules were analysed by LC–MS or the NAD/NADH-Glo kit (Promega).

To measure the k_{cat} and Michaelis constant, K_m, values, experiments were carried out with the same reagents and buffer as above. Adps activity was measured by detection of AMP generation using the AMP-Glo Assay (Promega). Values were calculated by varying ADPR concentration (4–256 µM) with a constant ATP concentration (100 µM) or by varying ATP concentration (8–256 µM) with a constant ADPR concentration (100 µM). Adps concentration in these experiments was 0.025 µM, and the reaction was incubated for 10 min at 25 °C and stopped by reagent 1 (AMP-Glo Assay).

Namat activity was measured by detection of NAD^+ generation using the NAD/NADH-Glo kit (Promega). Values were calculated by varying the nicotinamide concentration (0.0625–4 µM) with a constant concentration of ADPR (100 µM), or by varying the ADPR concentration (1–64 µM) with a constant concentration of nicotinamide (100 µM). The Namat concentration in these experiments was 0.015 µM, and the reaction was incubated for 10 min at 25 °C. All reactions for Namat were carried out in the presence of a high excess of Adps (0.5 µM) and ATP (500 µM), preincubated for 30 min at 25 °C with ADPR, to complete the transformation of ADPR to ADPR-PP, so that the ADPR-PP concentration was taken as equal to the ADPR concentration. All measurements were repeated three times. Steady-state kinetic parameters were evaluated by fitting the Michaelis–Menten or Hill equations to the data using the Enzyme_Kinetics_Calculator[47].

Enzymatic assay for AMP measurements

The AMP-Glo Assay (Promega) kit was used according to the manufacturer's protocol. A 5 µl volume of reaction mix was used for one measurement. The luciferase signal was detected using the Tecan Infinite 200 PRO plate reader. AMP concentrations were calculated from the calibration curve using a set of standard AMP samples with known concentrations.

Enzymatic assay for NAD^+ measurements

The NAD/NADH-Glo (Promega) kit was used for NAD^+ level measurement. The lysate or in vitro reactions were diluted 1:100 in 0.1 M Na-phosphate buffer, pH 8.0. Reactions were carried out in a volume of 10 µl (5 µl of sample + 5 µl of reaction mix) according to the manufacturer's protocol, and luciferase signal was detected using the Tecan Infinite 200 PRO plate reader every 2 min for 30 cycles. NAD^+ concentrations were calculated from the calibration curve using a set of standard NAD^+ samples with known concentrations.

Enzymatic treatment of ADPR-PP and ADPR-cP with apyrase and NudC

For apyrase treatment, 20 µl of reaction mixture of ADPR, ATP and Adps (Fig. 2d) was mixed with 15 µl of water, 4 µl of 10× apyrase buffer (NEB) and 1 µl of apyrase (M0398S, NEB), and then incubated for 30 min at 30 °C. Products were analysed by LC–MS.

For NudC treatment, 20 µl of reaction mixture of ADPR, ATP and Adps (Fig. 2d) was mixed with 13 µl of water, 4 µl of 10× r3.1 buffer (NEB), 2 µl of 100 µM dithiothreitol and 1 µl of NudC (M0607S, NEB), and then incubated for 30 min at 37 °C. Products were analysed by LC–MS.

Metabolite analysis through LC–MS

Metabolic profiling of the polar metabolites was carried out as described previously[48] with minor modifications as described below. In brief, analysis was carried out using an Acquity I class UPLC System combined with a mass spectrometer Q Exactive Plus Orbitrap (Thermo Fisher Scientific), which was operated in both positive and negative ionization modes. The LC separation was carried out using the SeQuant Zic-pHilic (150 mm × 2.1 mm) with the SeQuant guard column (20 mm × 2.1 mm; Merck). Mobile phase B was acetonitrile and mobile phase A was 20 mM ammonium carbonate with 0.1% ammonia hydroxide in deionized distilled water/acetonitrile (80:20, v/v). The flow rate was kept at 200 µl min^{-1}, and the gradient was as follows: 0–2 min 75% of B, 14 min 25% of B, 18 min 25% of B, 19 min 75% of B, for 4 min, 23 min 75% of B.

For the detection of NAD^+ and NMN by LC–MS, analysis was carried out by two separate injections in positive and negative ionization modes from m/z 75 to 1,000 at a mass resolution of 70,000. Peak areas were extracted using MZmine 2 with an accepted deviation of 5 ppm. In Fig. 2d, signals of all substrates were normalized to the signals of the

standard samples with the same concentration as used in the reaction. Signals for ADPR-PP and ADPR-cP were calculated from the decrease of used ADPR, because reactions were carried out with an excess ATP. All molecules used as standards were obtained from Sigma: ADPR (A0752), PRPP (P8296), D-RP (83875), ATP (A1852), nicotinamide (72340) NMN (N3501) and NAD^+ (N8285).

For detection of ADPR-PP and ADPR-cP, MS/MS spectra collection was carried out using the same instrument at a resolution of 17,500. Fragmentation was carried out through a higher-energy collisional dissociation cell using a normalized collision energy of 30. Fragments were extracted using MZmine 2.

Phylogenetic analyses of Adps and Namat

Homologues of Prs, Adps, Namat and Nmnat were searched for in 3,895 finished prokaryotic genomes (including 3,781 bacterial and 114 archaeal genomes)[1] downloaded in October 2017, as well as in 20,185 phage genomes from the INPHARED database downloaded on 1 May 2023[25]. For the Prs and Adps analysis, the *E. coli* Prs protein, phage Bas63 Adps and phage SpβL1 Adps were used as queries; for the Namat analysis, the Namat protein sequences from phages Bas63 and SpβL1 and Nampt from KVP40 were used. Nmnat was searched for using the sequence from phage KVP40 as a query. All proteins were searched for using the 'search' function of MMseqs2 (release 12-113e3)[41] using two iterations (parameter –num-iterations 2). Hits with an *e*-value lower than 10^{-5} were selected. Sequences from phage and prokaryotic genomes were separately filtered for redundancy by clustering sequences with identical length and at least 90% identity using the clust-hash option of MMseqs2[49]. Sequences shorter than 200 residues were discarded, and the remaining sequences were aligned using Clustal-Omega (v1.2.4)[50]. Phylogenetic trees were built using IQtree (v1.6.5)[51] with parameters -m LG -nt AUTO. Human PRPS1 and NAMPT were used as an outgroup for the Prs or Adps and Namat trees, respectively. Node support was computed using 1,000 iterations of the ultrafast bootstrap function in IQtree (option -bb 1000)[37]. All trees were visualized with iTOL[52]. For the Prs or Adps tree, leaves were annotated on the basis of the presence of a Namat homologue within ten genes upstream or downstream of Prs or Adps. For the Namat tree, each sequence was annotated on the basis of the presence of a Prs and Adps or Nmnat homologue in the same phage genome.

Reporting summary

Further information on research design is available in the Nature Portfolio Reporting Summary linked to this article.

Data availability

Data that support the findings of this study are available within the Article and Supplementary Tables 1–4. IMG and INPHARED accession numbers, protein sequences and nucleotide sequences are available in Supplementary Tables 1 and 2. Source data are provided with this paper.

38. Chung, C. T., Niemela, S. L. & Miller, R. H. One-step preparation of competent *Escherichia coli*: transformation and storage of bacterial cells in the same solution. *Proc. Natl Acad. Sci. USA* **86**, 2172–2175 (1989).
39. Doron, S. et al. Systematic discovery of antiphage defense systems in the microbial pangenome. *Science* **359**, eaar4120 (2018).
40. Hove-Jensen, B., Bentsen, A. K. & Harlow, K. W. Catalytic residues Lys197 and Arg199 of *Bacillus subtilis* phosphoribosyl diphosphate synthase. Alanine-scanning mutagenesis of the flexible catalytic loop. *FEBS J.* **272**, 3631–3639 (2005).
41. Eriksen, T. A., Kadziola, A., Bentsen, A. K., Harlow, K. W. & Larsen, S. Structural basis for the function of *Bacillus subtilis* phosphoribosyl-pyrophosphate synthetase. *Nat. Struct. Biol.* **7**, 303–308 (2000).
42. Adler, B. A. et al. Broad-spectrum CRISPR-Cas13a enables efficient phage genome editing. *Nat. Microbiol.* **7**, 1967–1979 (2022).
43. Leavitt, A. et al. Viruses inhibit TIR gcADPR signalling to overcome bacterial defence. *Nature* **611**, 326–331 (2022).
44. Baba, T. et al. Construction of *Escherichia coli* K-12 in-frame, single-gene knockout mutants: the Keio collection. *Mol. Syst. Biol.* **2**, 2006.0008 (2006).
45. Thomason, L. C., Costantino, N. & Court, D. L. *E. coli* genome manipulation by P1 transduction. *Curr. Protoc. Mol. Biol.* **79**, 1.17.1–1.17.8 (2007).
46. Mazzocco, A., Waddell, T. E., Lingohr, E. & Johnson, R. P. Enumeration of bacteriophages using the small drop plaque assay system. *Methods Mol. Biol.* **501**, 81–85 (2009).
47. Kitaoka, M. Automatic calculation of the kinetic parameters of enzymatic reactions with their standard errors using Microsoft Excel. *J. Appl. Glycosci.* **70**, 33–37 (2023).
48. Zheng, L. et al. Fumarate induces redox-dependent senescence by modifying glutathione metabolism. *Nat. Commun.* **6**, 6001 (2015).
49. Steinegger, M. & Soding, J. MMseqs2 enables sensitive protein sequence searching for the analysis of massive data sets. *Nat. Biotechnol.* **35**, 1026–1028 (2017).
50. Sievers, F. et al. Fast, scalable generation of high-quality protein multiple sequence alignments using Clustal Omega. *Mol. Syst. Biol.* **7**, 539 (2011).
51. Nguyen, L. T., Schmidt, H. A., von Haeseler, A. & Minh, B. Q. IQ-TREE: a fast and effective stochastic algorithm for estimating maximum-likelihood phylogenies. *Mol. Biol. Evol.* **32**, 268–274 (2015).
52. Letunic, I. & Bork, P. Interactive Tree Of Life (iTOL) v4: recent updates and new developments. *Nucleic Acids Res.* **47**, W256–W259 (2019).

Acknowledgements We thank members of the laboratory of R.S. for comments on earlier versions of this manuscript. R.S. was supported, in part, by the European Research Council (grant number ERC-AdG GA 101018520), the Israel Science Foundation (MAPATS grant 2720/22), the Deutsche Forschungsgemeinschaft (SPP 2330, grant 464312965), a research grant from the Estate of Marjorie Plesset, the Ernest and Bonnie Beutler Research Program of Excellence in Genomic Medicine, the Dr. Barry Sherman Institute for Medicinal Chemistry, M.de Botton, the Andre Deloro Prize and the Knell Family Center for Microbiology. I.O. was supported by the Ministry of Absorption New Immigrant programme. E.Y. is supported by the Clore Scholars Program, and, in part, by the Israeli Council for Higher Education through the Weizmann Data Science Research Center.

Author contributions The study was conceptualized and designed by I.O. and R.S. I.O. conducted all phage knockout and knock-in experiments, tested the anti-defence effect of NARP1, purified Adps and Namat proteins and carried out all in vitro experiments. H.S. cloned and measured the anti-defence effect of NARP2. F.R. carried out a phylogenetic analysis of Adps and Namat. E.L. collected and processed samples for LC–MS. M.I. and S.M. carried out all LC–MS experiments. E.Y. identified phages with NARP1 in laboratory phage collection. A.M. collected sequences of Prs and Nampt genes in bacterial and phage genomes. The manuscript was written by I.O. and R.S. All authors contributed to editing the manuscript and support the conclusions.

Competing interests R.S. is a scientific cofounder and adviser of BiomX and Ecophage. The other authors declare no competing interests.

Additional information

Supplementary information The online version contains supplementary material available at https://doi.org/10.1038/s41586-024-07986-w.

Correspondence and requests for materials should be addressed to Ilya Osterman or Rotem Sorek.

Peer review information *Nature* thanks Charles Brenner, Hening Lin and Malcolm White for their contribution to the peer review of this work.

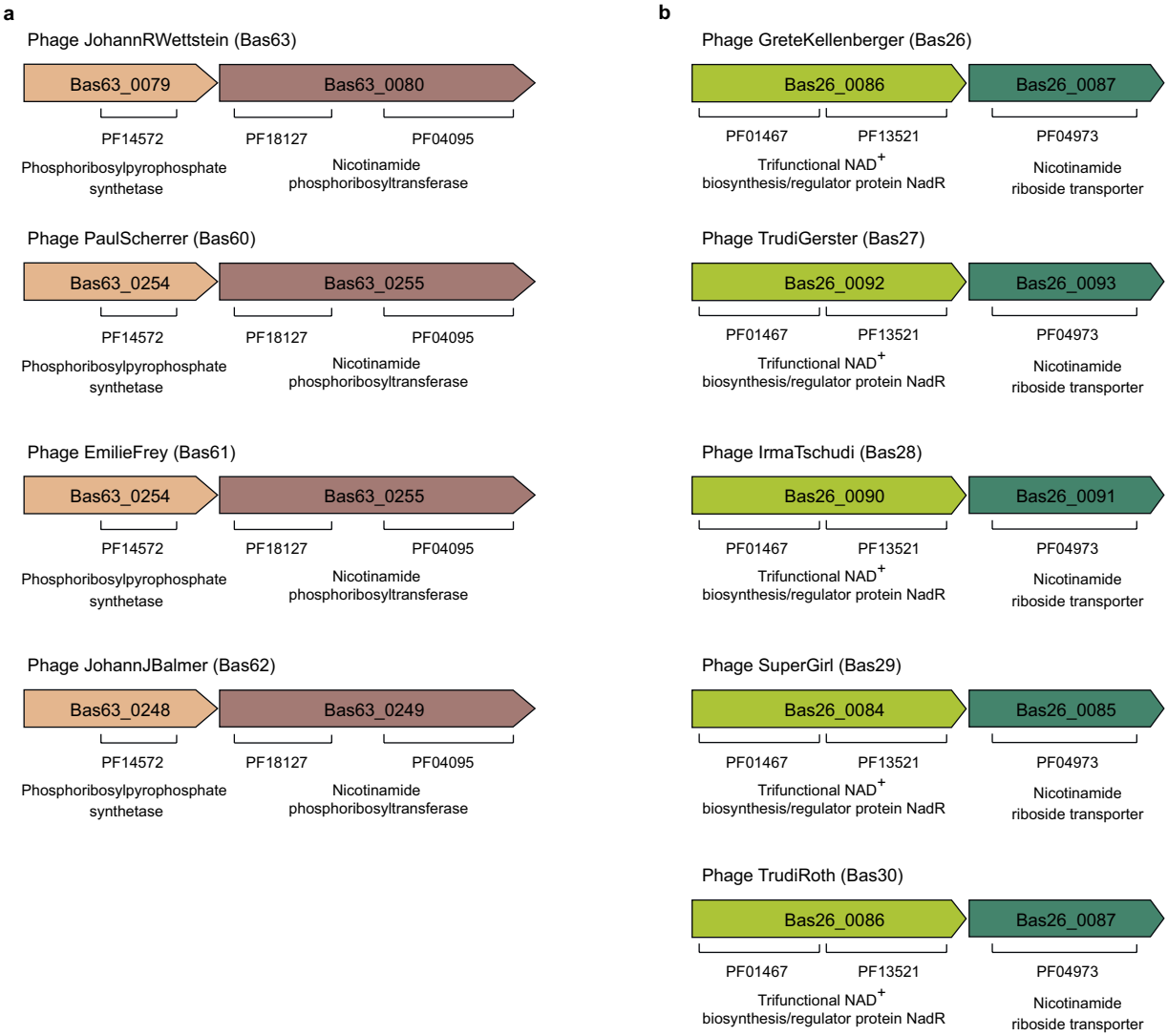

Extended Data Fig. 1 | BASEL-collection phages encoding NAD reconstitution pathways. a. BASEL-collection phages that encode the NARP1 pathway. **b**. BASEL-collection phages that encode a two-gene operon predicted to comprise NadR and a transporter for nicotinamide riboside. This operon is hypothesized to comprise a phage NAD^+ reconstitution pathway that was not examined in the current study.

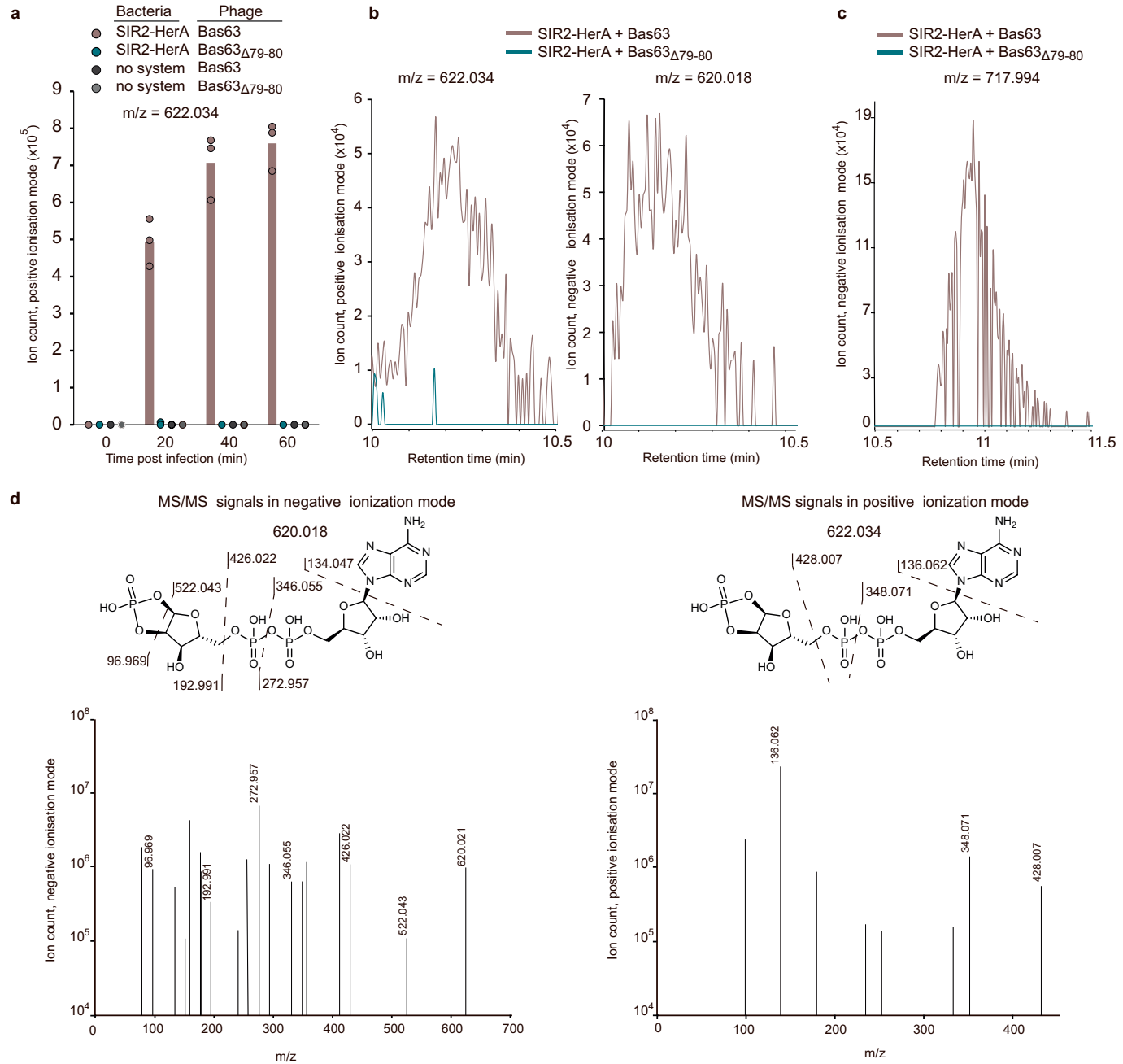

Extended Data Fig. 2 | Mass spectrometry analysis of metabolites detected in lysates from infected cells. a. A unique molecule with an m/z value of 622.034 appears in SIR2-HerA cells infected by Bas63. Cells were infected at MOI = 10. Bars represent the mean area under the curve (AUC) of three experiments, with individual data points overlaid. **b**. Extracted mass chromatograms of ions with an m/z value of 622.034 (positive ionization mode) and 620.021 (negative ionization mode) and retention time of 10.2 min. **c**. MS data in negative ionization mode for the same molecule presented in Fig. 2b. **d**. MS/MS fragmentation spectra of the molecule with the m/z value 620.021 (negative ionization mode) and 622.034 (positive ionization mode). The hypothesized structure of the molecule and MS/MS fragments are presented.

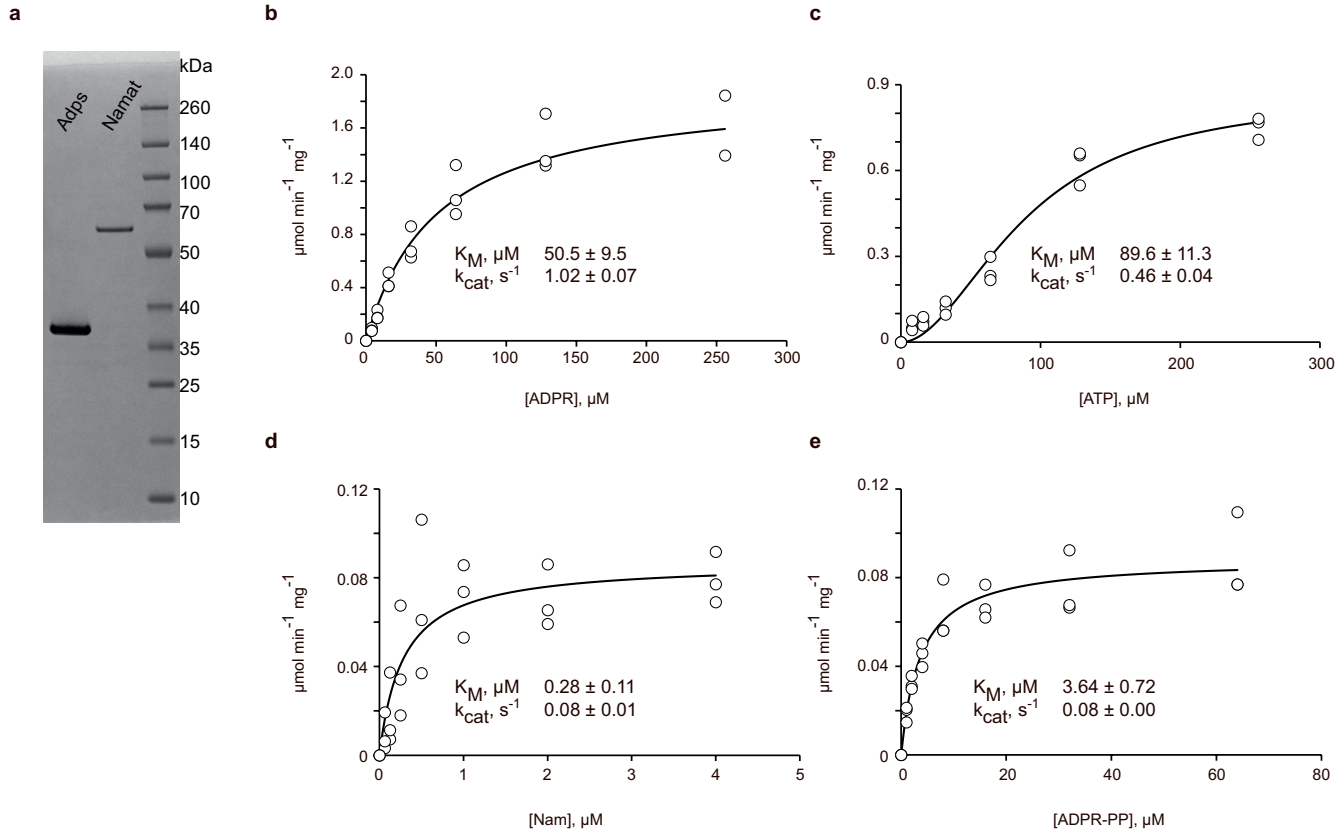

Extended Data Fig. 3 | Characterization of the Adps and Namat enzymes. **a**. An SDS-PAGE gel showing the purified Adps (predicted Mw of 32.1 kDa including the 6xhis tag) and Namat (56.6 kDa including the 6xhis tag). For gel source data, see Supplementary Fig. 1. **b**. A plot of the velocity (µmol*min^{-1}*mg^{-1}) of AMP production by Adps in various concentrations of ADPR in the presence of 100 µM ATP. **c**. A plot of the velocity (µmol*min^{-1}*mg^{-1}) of AMP production by Adps in various concentrations of ATP in the presence of 100 µM ADPR. In both panels **b** and **c**, the appearance of AMP was measured by the AMP-Glo assay (Promega) **d**. A plot of the velocity (µmol*min^{-1}*mg^{-1}) of NAD production by Namat in various concentrations of nicotinamide in the presence of 100 µM ADPR-PP. **e**. A plot of the velocity (µmol*min^{-1}*mg^{-1}) of NAD production by Namat in various concentrations of ADPR-PP in the presence of 100 µM nicotinamide. Steady-state kinetic parameters were evaluated by fitting the Michaelis-Menten or Hill equations to data generated by 3 independent measurements using the Enzyme_Kinetics_Calculator[47]. Individual data points are overlaid on the curves.

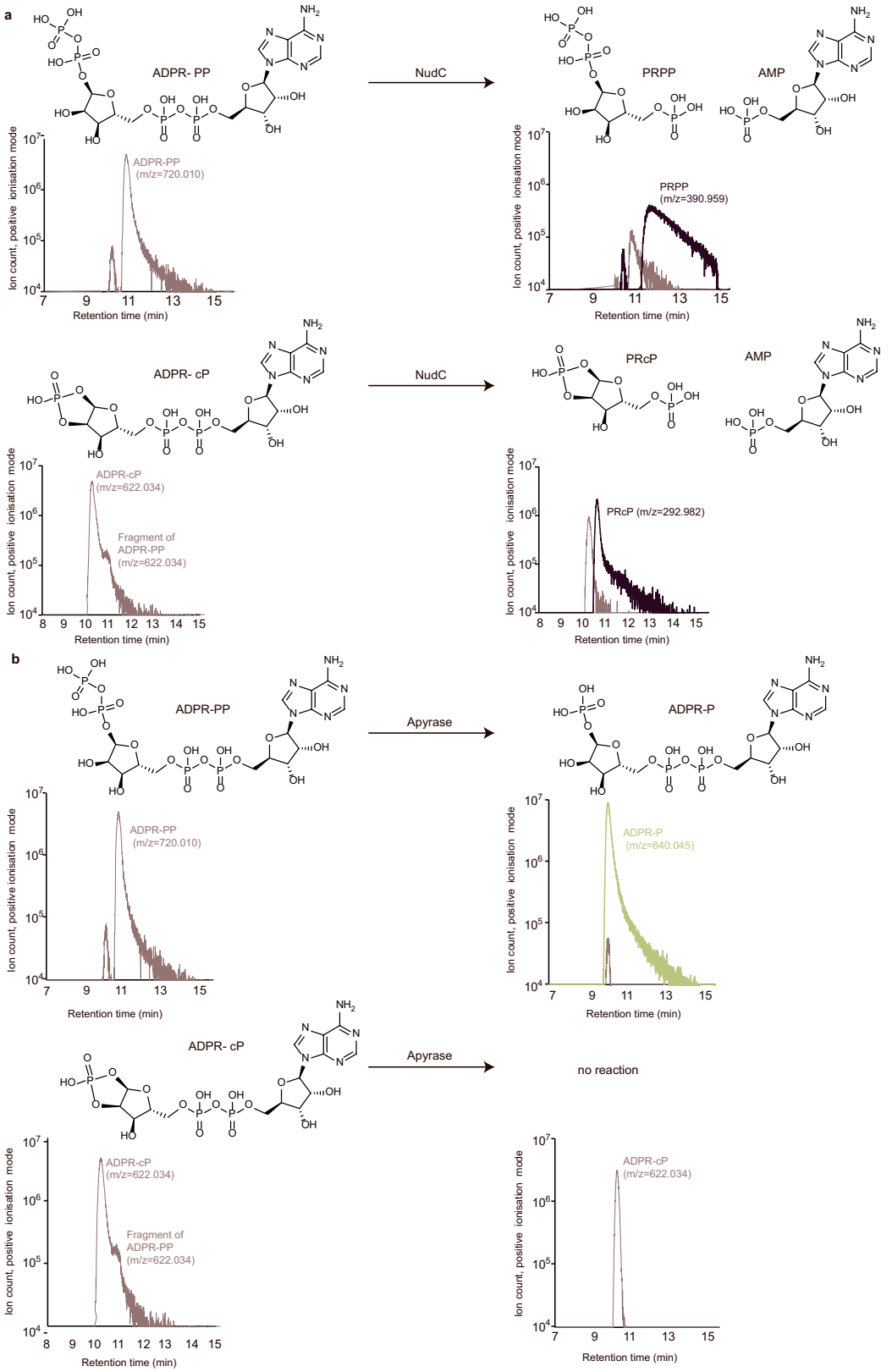

Extended Data Fig. 4 | Enzymatic treatment of NARP1 products. **a**. Schematic of the reactions and mass-chromatograms of ADPR-PP and ADPR-cP following incubation with the enzyme NudC. Representative chromatograms of three replicates are presented. **b**. Schematic of the reactions and mass-chromatograms of ADPR-PP and ADPR-cP following incubation with the enzyme Apyrase. The peak with m/z 622.034 and retention time 11.0 is hypothesized to correspond to fragmentation of ADPR-PP by ionization in mass spectrometer. Representative chromatograms of three replicates are presented.

nature portfolio

Corresponding author(s): Ilya Osterman, Rotem Sorek

Last updated by author(s): Aug 4, 2024

Reporting Summary

Nature Portfolio wishes to improve the reproducibility of the work that we publish. This form provides structure for consistency and transparency in reporting. For further information on Nature Portfolio policies, see our Editorial Policies and the Editorial Policy Checklist.

Statistics

For all statistical analyses, confirm that the following items are present in the figure legend, table legend, main text, or Methods section.

n/a	Confirmed	
☐	☒	The exact sample size (*n*) for each experimental group/condition, given as a discrete number and unit of measurement
☐	☒	A statement on whether measurements were taken from distinct samples or whether the same sample was measured repeatedly
☐	☒	The statistical test(s) used AND whether they are one- or two-sided *Only common tests should be described solely by name; describe more complex techniques in the Methods section.*
☒	☐	A description of all covariates tested
☒	☐	A description of any assumptions or corrections, such as tests of normality and adjustment for multiple comparisons
☐	☒	A full description of the statistical parameters including central tendency (e.g. means) or other basic estimates (e.g. regression coefficient) AND variation (e.g. standard deviation) or associated estimates of uncertainty (e.g. confidence intervals)
☒	☐	For null hypothesis testing, the test statistic (e.g. *F*, *t*, *r*) with confidence intervals, effect sizes, degrees of freedom and *P* value noted *Give P values as exact values whenever suitable.*
☒	☐	For Bayesian analysis, information on the choice of priors and Markov chain Monte Carlo settings
☒	☐	For hierarchical and complex designs, identification of the appropriate level for tests and full reporting of outcomes
☒	☐	Estimates of effect sizes (e.g. Cohen's *d*, Pearson's *r*), indicating how they were calculated

Our web collection on statistics for biologists contains articles on many of the points above.

Software and code

Policy information about availability of computer code

Data collection	No software was used for data collection
Data analysis	MMseqs2 (release 12-113e3), Clustal-Omega 1.2.4, IQ-TREE 1.6.5, iTOL 6.8.1, MZmine 2

For manuscripts utilizing custom algorithms or software that are central to the research but not yet described in published literature, software must be made available to editors and reviewers. We strongly encourage code deposition in a community repository (e.g. GitHub). See the Nature Portfolio guidelines for submitting code & software for further information.

Data

Policy information about availability of data

All manuscripts must include a data availability statement. This statement should provide the following information, where applicable:

- Accession codes, unique identifiers, or web links for publicly available datasets
- A description of any restrictions on data availability
- For clinical datasets or third party data, please ensure that the statement adheres to our policy

Data that support the findings of this study are available within the article and its Supplementary Tables 1-4. IMG/INPHARED accessions, protein sequences and nucleotide sequences appear in Supplementary Tables 1 and 2. Source data are available for all the main figures and for extended data figures 2, 3 and 4.

Research involving human participants, their data, or biological material

Policy information about studies with human participants or human data. See also policy information about sex, gender (identity/presentation), and sexual orientation and race, ethnicity and racism.

Reporting on sex and gender	N/A
Reporting on race, ethnicity, or other socially relevant groupings	N/A
Population characteristics	N/A
Recruitment	N/A
Ethics oversight	N/A

Note that full information on the approval of the study protocol must also be provided in the manuscript.

Field-specific reporting

Please select the one below that is the best fit for your research. If you are not sure, read the appropriate sections before making your selection.

☒ Life sciences ☐ Behavioural & social sciences ☐ Ecological, evolutionary & environmental sciences

For a reference copy of the document with all sections, see nature.com/documents/nr-reporting-summary-flat.pdf

Life sciences study design

All studies must disclose on these points even when the disclosure is negative.

Sample size	Experiments were performed in triplicates without prior sample size calculation (unless mentioned otherwise), as is standard for such experimental designs
Data exclusions	No data were excluded from the analyses
Replication	Experiments were performed in triplicates. No failed replications occurred.
Randomization	Randomization was not performed in the study because it was determined that the study design and objectives did not require it.
Blinding	Blinding was not required in this study as data were collected using highly quantitative measures over multiple independent replicates.

Reporting for specific materials, systems and methods

We require information from authors about some types of materials, experimental systems and methods used in many studies. Here, indicate whether each material, system or method listed is relevant to your study. If you are not sure if a list item applies to your research, read the appropriate section before selecting a response.

Materials & experimental systems

n/a	Involved in the study
☒	☐ Antibodies
☒	☐ Eukaryotic cell lines
☒	☐ Palaeontology and archaeology
☒	☐ Animals and other organisms
☒	☐ Clinical data
☒	☐ Dual use research of concern
☒	☐ Plants

Methods

n/a	Involved in the study
☒	☐ ChIP-seq
☒	☐ Flow cytometry
☒	☐ MRI-based neuroimaging

Plants

Seed stocks

Report on the source of all seed stocks or other plant material used. If applicable, state the seed stock centre and catalogue number. If plant specimens were collected from the field, describe the collection location, date and sampling procedures.

Novel plant genotypes

Describe the methods by which all novel plant genotypes were produced. This includes those generated by transgenic approaches, gene editing, chemical/radiation-based mutagenesis and hybridization. For transgenic lines, describe the transformation method, the number of independent lines analyzed and the generation upon which experiments were performed. For gene-edited lines, describe the editor used, the endogenous sequence targeted for editing, the targeting guide RNA sequence (if applicable) and how the editor was applied.

Authentication

Describe any authentication procedures for each seed stock used or novel genotype generated. Describe any experiments used to assess the effect of a mutation and, where applicable, how potential secondary effects (e.g. second site T-DNA insertions, mosiacism, off-target gene editing) were examined.